



QED with a parabolic mirror

G. Alber,¹ J. Z. Bernád,¹ M. Stobińska,^{2,3} L. L. Sánchez-Soto,^{4,5,6} and G. Leuchs^{4,5}

¹*Institut für Angewandte Physik, Technische Universität Darmstadt, 64289 Darmstadt, Germany*

²*Institute of Theoretical Physics and Astrophysics, University of Gdańsk, ul. Wita Stwosza 57, 80-952 Gdańsk, Poland*

³*Institute of Physics, Polish Academy of Sciences, Al. Lotników 32/46, 02-668 Warsaw, Poland*

⁴*Max-Planck-Institut für die Physik des Lichts, Günther-Scharowsky-Straße 1, Bau 24, 91058 Erlangen, Germany*

⁵*Department für Physik, Universität Erlangen-Nürnberg, Staudtstraße 7, Bau 2, 91058 Erlangen, Germany*

⁶*Departamento de Óptica, Facultad de Física, Universidad Complutense, 28040 Madrid, Spain*

(Received 11 May 2013; published 14 August 2013)

We investigate the quantum electrodynamics of a single two-level atom located at the focus of a parabolic cavity. We first work out the modifications of the spontaneous emission induced by the presence of this boundary in the optical regime, where the dipole and the rotating-wave approximations apply. Furthermore, the single-photon state that leaves the cavity asymptotically is determined. The corresponding time-reversed single-photon quantum state is capable of exciting the atom in this extreme multimode scenario with near-unit probability. Using semiclassical methods, we derive a photon-path representation for the relevant transition amplitudes and show that it constitutes a satisfactory approximation for a wide range of wavelengths.

DOI: [10.1103/PhysRevA.88.023825](https://doi.org/10.1103/PhysRevA.88.023825)

PACS number(s): 42.50.Pq, 42.50.Ct, 42.50.Ar, 42.50.Ex

I. INTRODUCTION

The physics of strong light-matter coupling has been attracting a great deal of attention over the last few years. Since the early eighties, single atoms have been coupled to optical and microwave cavities, leading to fundamental demonstrations of cavity quantum electrodynamics (QED) [1–3]. More recently, impressive developments in circuit QED [4], involving superconducting qubits coupled to microwave cavities, atom chips [5], and chip-based microresonators [6] have opened the door to the ultrastrong coupling regime, holding the promise to exploit light-matter interaction at the single-photon level in scalable architectures. This is of pivotal significance for future applications of quantum technologies.

Thus far, in typical cavity QED configurations, the atomic properties are considerably changed because the cavity boundaries modify the electromagnetic mode structure [7]. Actually, the radiating atom can excite only one or a few radiation modes [8]. In these cases, we can observe spontaneous emission enhancement or inhibition into the modes that are resonant or nonresonant with the cavity, respectively.

The extreme opposite regime of free-space QED, where a continuum of modes is available, has also received notable recognition [9], motivated by the hope of finding simpler solutions for quantum communication over large distances. In these circumstances, it is essential to increase the strength of the light-matter interaction: strongly focused light improves the coupling [10] and matching the incoming field with the spatial atomic radiation mode improves focusing [11]. Moreover, tailoring the polarization pattern can be significant for achieving near perfect coupling [12].

An intriguing intermediate instance between the single-mode and the continuum limit is the case of a large cavity [13–15], in which an atom couples to a large but not continuous number of modes. A half cavity, i.e., a cavity with one mirror, constitutes a good example of such a situation [16,17]. It has been verified experimentally that also in this regime one can witness a change of the density

of field modes near an atom, which manifests in a modified spontaneous-emission rate [18,19].

A parabolic cavity is a remarkable example of a half cavity. The parabolic shape ensures that light entering parallel to the symmetry axis couples to an atom located at its focus in a particularly efficient way, the light impinging on the atom from all directions [20]. Conversely, such a parabola collects the light emitted by an atom in the spontaneous decay in all directions.

In a classical ray picture, valid for focal lengths of the parabola large in comparison with the relevant wavelengths of the radiation, only the small fraction of radiation emitted by the atom along the symmetry axis in the direction of the vertex of the parabola is back-reflected towards the atom. Thus, it might seem that the atom scarcely feels the presence of boundaries. However, this picture is largely oversimplified: if the focal length becomes comparable to the relevant wavelengths, diffraction effects become important and significant modifications of the spontaneous emission can be expected. Besides, the atom is not a point, but it scatters photons within a region whose linear extension is of the order of the wavelength. Thus, both diffraction and resonant photon scattering by the atom are expected to modify the simple short-wavelength picture substantially.

Prompted by the current interest in radiative effects in half-open cavities, we look here into the QED of a two-level atom located at the focus of a parabolic mirror. First, we find the vector field modes that can couple efficiently to the atom in the dipole approximation. In terms of them, we study the ensuing modifications of the spontaneous emission as well as the quantum statistical space-time properties of the generated photon.

For that purpose, we develop a semiclassical path representation of probability amplitudes that interpret them as sums of contributions associated with different photon paths inside the parabolic cavity. Exploiting in a systematic way the separability of the Helmholtz equation in parabolic coordinates, such a representation provides an adequate quantitative description of the spontaneous emission, not only in the short-wavelength

limit, but also in the regime of wavelengths comparable or even smaller than the focal length of the cavity.

The plan of this paper is as follows. In Sec. II the basic model and the approximations involved are summarized. The dynamics of the spontaneous decay process is described in Sec. III: the decay rate and its dependence on the focal length is discussed in Sec. III A, while the subsequent subsection explores the conditions under which the spontaneous emission can be described by an exponential decay and the modifications that occur due to the presence of the cavity. Finally, in Sec. IV characteristic properties of the spontaneously generated one-photon quantum state are discussed.

II. SETTING THE MODEL

A. Atom-field interaction in a parabolic mirror

We consider an atom situated at the focus \mathbf{x}_0 of an axially symmetric parabolic cavity, as sketched in Fig. 1. We take the atom initially prepared in an excited electronic state, say $|e\rangle$, that decays to the ground state $|g\rangle$ via an allowed dipole transition. In the Schrödinger picture, we can model this atom by a two-level system with the Hamiltonian

$$\hat{H}_A = E_e|e\rangle\langle e| + E_g|g\rangle\langle g|. \quad (2.1)$$

The free evolution of the quantized radiation field inside this cavity is described by

$$\hat{H}_F = \sum_n \int d\omega \hbar\omega \hat{a}_{\omega,n}^\dagger \hat{a}_{\omega,n}, \quad (2.2)$$

which has to include all the modes which couple quasiresonantly to the atom. These modes (whose explicit form will be determined in the next subsection) are labeled by their continuous frequencies ω and by a discrete parameter n that incorporates the boundary effects. In Eq. (2.2), $\hat{a}_{\omega,n}^\dagger$ and $\hat{a}_{\omega,n}$ are the creation and destruction operators of the corresponding modes, respectively.

We recall that, in the Schrödinger picture, the operators of the electric field $\hat{\mathbf{E}}(\mathbf{x})$ and of the magnetic field $\hat{\mathbf{B}}(\mathbf{x})$ of these

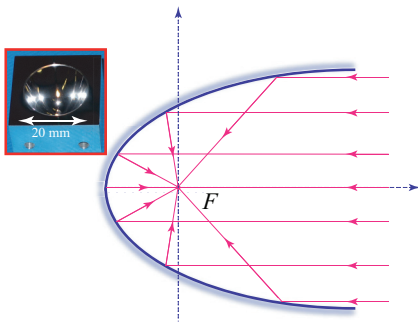


FIG. 1. (Color online) Schematic representation of the parabolic cavity: the two-level atom is situated at the focus F (which is taken as $\mathbf{x}_0 = 0$). In parabolic coordinates the boundary of this cavity is given by the equation $\eta = 2f$. We also include a picture of the real mirror in the Erlangen experiment, with focal length of $f = 2.1$ mm and a front opening of 20 mm in diameter.

modes are given by

$$\begin{aligned} \hat{\mathbf{E}}(\mathbf{x}) &= i\sqrt{\frac{\hbar\omega}{2\epsilon_0}} \sum_n \int_0^\infty d\omega [\mathbf{g}_{\omega,n}(\mathbf{x}) \hat{a}_{\omega,n} - \text{H. c.}], \\ \hat{\mathbf{B}}(\mathbf{x}) &= \sqrt{\frac{\hbar\omega}{2\epsilon_0}} \sum_n \int_0^\infty d\omega [\nabla \times \mathbf{g}_{\omega,n}(\mathbf{x}) \hat{a}_{\omega,n} + \text{H. c.}], \end{aligned} \quad (2.3)$$

with H. c. denoting the Hermitian conjugate operators. The orthonormal mode functions $\mathbf{g}_{\omega,n}(\mathbf{x})$ fulfill the transversality condition $\nabla \cdot \mathbf{g}_{\omega,n}(\mathbf{x}) = 0$ and they are solutions of the vectorial Helmholtz equation

$$\left(\nabla^2 + \frac{\omega^2}{c^2}\right) \mathbf{g}_{\omega,n}(\mathbf{x}) = 0, \quad (2.4)$$

with c the speed of light in vacuum. This equation has to be interpreted in the sense that it applies to each Cartesian component of the mode function separately. The orthonormality condition reads

$$\int_{\mathbb{R}^3} d^3\mathbf{x} \mathbf{g}_{\omega,n}^*(\mathbf{x}) \cdot \mathbf{g}_{\omega',n'}(\mathbf{x}) = \delta_{nn'} \delta(\omega - \omega'). \quad (2.5)$$

In the dipole approximation, the atom-field interaction is described by $-\hat{\mathbf{d}} \cdot \hat{\mathbf{E}}(\mathbf{x}_0)$, with $\hat{\mathbf{d}}$ being the atomic dipole operator. In the optical range, where the rotating-wave approximation is valid, this coupling reduces to

$$\hat{H}_{AF} = -i\sqrt{\frac{\hbar\omega}{2\epsilon_0}} \sum_n \int d\omega [\mathbf{d} \cdot \mathbf{g}_{\omega,n}(\mathbf{x}_0) \hat{a}_{\omega,n} |e\rangle\langle g| + \text{H. c.}], \quad (2.6)$$

where $\mathbf{d} = \langle e|\hat{\mathbf{d}}|g\rangle$ is the atomic-dipole matrix element between the excited $|e\rangle$ and the ground state $|g\rangle$.

To assess the dynamics of the spontaneous emission, one has to solve the time-dependent Schrödinger equation with the Hamiltonian

$$\hat{H} = \hat{H}_A + \hat{H}_F + \hat{H}_{AF} \quad (2.7)$$

and the initial condition that at time t_0 the state of the atom-field system is

$$|\psi(t_0)\rangle = |e\rangle \otimes |0\rangle, \quad (2.8)$$

$|0\rangle$ being the ground (vacuum) state of the free electromagnetic field.

B. Normal modes and quantization

We assume the two-level atom located at the focus of the parabolic cavity (which we take as $\mathbf{x}_0 = 0$), with its transition dipole matrix element \mathbf{d} oriented along the symmetry axis of the parabola, i.e., $\mathbf{d} = d\mathbf{e}_3$ for this is the case in the experimental setup in our laboratory [21]. As a result, this atom couples exclusively to those modes whose electric field at the focus is oriented along the symmetry axis. For distances close to the atom ($|\mathbf{x} - \mathbf{x}_0|/\omega/c \ll 1$), these mode functions are not modified by the boundary conditions and are of the same form as in free space, i.e.,

$$\mathbf{g}_{\omega,n}(\mathbf{x}) \rightarrow \nabla \times C\rho\mathbf{e}_\varphi = 2C\mathbf{e}_3, \quad (2.9)$$

where C is a normalization constant and we have used cylindrical coordinates (ρ, φ, z) . The vector $\mathbf{e}_\varphi = \cos \varphi \mathbf{e}_2 - \sin \varphi \mathbf{e}_1$ denotes the unit tangent vector in the angular direction φ .

Far away from the atom, however, these modes are altered by the presence of the parabola. Transversality can be ensured by imposing

$$\mathbf{g}_{\omega,n}(\mathbf{x}) = \nabla \times \mathbf{G}_{\omega,n}(\mathbf{x}), \quad (2.10)$$

so that $\mathbf{G}(\mathbf{x}) = f(x,y)\mathbf{e}_\varphi$ is also a solution of the Helmholtz equation.

The separability of that equation in parabolic coordinates, suggests the ansatz (see the Appendix)

$$\mathbf{G}_{\omega,n}(\mathbf{x}) = \frac{1}{\sqrt{2\pi\omega\mathcal{N}_{\omega,n}}} \frac{\chi_{\omega,n}(\xi)}{\sqrt{\xi}} \frac{\chi_{\omega,n}(\eta)}{\sqrt{\eta}} \mathbf{e}_\varphi, \quad (2.11)$$

provided the regular functions $\chi_{\omega,n}(\xi)$ and $\chi_{\omega,n}(\eta)$ fulfill

$$\begin{aligned} \left(\frac{d^2}{d\xi^2} + \frac{\omega^2}{4c^2} - \frac{\alpha}{\xi} \right) \chi_{\omega,n}(\xi) &= 0, \\ \left(\frac{d^2}{d\eta^2} + \frac{\omega^2}{4c^2} + \frac{\alpha}{\eta} \right) \chi_{\omega,n}(\eta) &= 0. \end{aligned} \quad (2.12)$$

For each frequency ω , the possible values α_n of the separation constant $-\infty < \alpha < \infty$ have to be determined by the boundary conditions at the surface of the parabola. The frequency-normalized solutions of Eqs. (2.12) can be expressed in terms of the Coulomb functions $F_L(\mu, \rho)$ [22]

$$\begin{aligned} \chi_{\omega,n}(\xi) &= \sqrt{\frac{4}{\pi k}} F_0(\alpha_n/k, k\xi/2), \\ \chi_{\omega,n}(\eta) &= \sqrt{\frac{4}{\pi k}} F_0(-\alpha_n/k, k\eta/2), \end{aligned} \quad (2.13)$$

with $k := \omega/c$. In lieu of this procedure, one could also find $\mathbf{G}_{\omega,n}(\mathbf{x})$ from the general solution of the scalar Helmholtz equation in parabolic coordinates worked out in Ref. [23] by imposing the Coulomb gauge condition and the appropriate boundary condition at a later stage. However, in general such an approach may lead to formidable mathematical problems.

In these coordinates, the parabola of focal length f is given by the equation $\eta = 2f$, so the normalization factor in Eq. (2.11) reads

$$\mathcal{N}_{\omega,n} = \int_0^{2f} d\eta \frac{\chi_{\omega,n}^2(\eta)}{\eta}, \quad (2.14)$$

and has been chosen in such a way that the mode function $\mathbf{g}_{\omega,n}(\mathbf{x})$ satisfies the condition (2.5).

The quantization of the separation constant α is determined by the boundary conditions at the surface of the parabola. To simplify the details as much as possible, we take a perfect metallic mirror with no losses and reflection coefficient $r = -1$ (we neglect any dependence of r on the angle of incidence or on the wavelength). This corresponds to imposing the tangential components of the electric field and the normal component of the magnetic field to vanish, which is warranted whenever

$$\left. \frac{d\chi_{\omega,n}}{d\eta} \right|_{\eta=2f} = 0, \quad (2.15)$$

wherefrom the permitted values α_n can be determined for each possible frequency ω and for $n \in \mathbb{N}$.

In the semiclassical limit, $\chi_{\omega,n}^2(\eta)$ is a rapidly oscillating function over the range of integration in Eq. (2.14). The quantization condition can be encoded in an eikonal function $S(\omega, \alpha) = \pi[n(\omega, \alpha) + 1/2]$ and the normalization factor fulfills the characteristic relation

$$\mathcal{N}_{\omega,n} = 2 \frac{\partial n}{\partial \alpha}(\omega, \alpha_n), \quad (2.16)$$

which establishes an important relation between the separation constant α and the quantization number n . We underline that for the setup in our laboratory in Erlangen, where $f = 2.1$ mm and a wavelength of 369 nm is used, this semiclassical limit is well satisfied.

III. QED EFFECTS AT THE FOCUS OF A PARABOLIC MIRROR

In this section, we first discuss the dependence of the spontaneous decay rate $\Gamma(\omega_0)$ on the focal length f of the parabola in the framework of a time-dependent perturbation theory.

The second subsection is devoted to an investigation of the dynamics of the spontaneous emission. In particular, we demonstrate that for moderate focal lengths the spontaneous decay is exponential, whereas, if the focal length is large enough so that subsequent reflections of the photon at the parabola can be distinguished in space-time, this exponential decay is appreciably modified.

For the quantitative analysis of this latter phenomenon a photonic semiclassical path representation is developed. In the spirit of the path integral approach [24], it resolves the probability amplitudes of interest into contributions corresponding to all possible photon paths and their multiple reflections at the parabolic mirror. This picture also sheds light onto the validity of the pole approximation [25].

A. The spontaneous decay rate

The spontaneous decay rate characterizes the basic aspects of the spontaneous emission of a photon of frequency $\omega_0 = (E_e - E_g)/\hbar$. In the dipole approximation and in the lowest order of time-dependent perturbation theory [26], it is given by

$$\Gamma(\omega_0) = \frac{2\pi}{\hbar^2} \sqrt{\frac{\hbar\omega_0}{2\epsilon_0}} \sum_n |\mathbf{d} \cdot \mathbf{g}_{\omega_0,n}(\mathbf{x}_0)|^2. \quad (3.1)$$

Using the mode functions $\mathbf{g}_{\omega,n}(\mathbf{x})$ we obtain for our case

$$\Gamma(\omega_0) = \Gamma_s(\omega_0) \frac{6}{\pi k_0} \sum_n \frac{1}{\mathcal{N}_{\omega_0,n}} \left(\frac{\pi \alpha_n(\omega_0)/k_0}{\sinh[\pi \alpha_n(\omega_0)/k_0]} \right)^2, \quad (3.2)$$

with $k_0 = \omega_0/c$ and

$$\Gamma_s(\omega_0) = \frac{|\mathbf{d}|^2 \omega_0^3}{3\pi \epsilon_0 \hbar c^3} \quad (3.3)$$

is the free-space spontaneous decay rate. Equation (3.2) conveys all the modifications in the spontaneous emission

brought about by the parabolic mirror. As we can see, it involves a sum over all the quantized separation constants $\alpha_n(\omega_0)$, which makes its explicit evaluation difficult, except if only a few values of the separation constants $\alpha_n(\omega_0)$ contribute dominantly to the summation.

Alternatively, we can rewrite Eq. (3.2) making use of the semiclassical relation (2.16) and of the Poisson summation formula [27] as

$$\Gamma(\omega_0) = \Gamma_s(\omega_0) \sum_{M=-\infty}^{\infty} \frac{3}{\pi^2} \int_{-\infty}^{\infty} dx \frac{x^2}{\sinh^2 x} \times \exp[i2\pi Mn(\omega_0, x)], \quad (3.4)$$

where $x := \pi\alpha_n(\omega_0)/k_0$. This form is particularly convenient if the exponential functions involved in the integration over x are rapidly oscillating functions. In these cases, the dominant contribution of Eq. (3.4) comes from the term with $M = 0$, which yields precisely 1. Consequently, if the contributions to Eq. (3.4) resulting from $M \neq 0$ are neglected, the spontaneous decay rate $\Gamma(\omega_0)$ reduces to its value in free space $\Gamma_s(\omega_0)$.

The effective range of integration in Eq. (3.4) is centered around $x = 0$ with a width $\Delta x = O(1)$. For $x = 0$, the mode function $\chi_{\omega,0}(\eta)$ and the normalization constant $\mathcal{N}_{\omega,0}$ are known exactly [22], namely,

$$\chi_{\omega,0}(\eta) = \sqrt{\frac{4}{\pi k}} \sin(k\eta/2), \quad (3.5)$$

$$\mathcal{N}_{\omega,0} = \frac{4}{\pi k} \int_0^{2f} d\eta \frac{\sin^2(k\eta/2)}{\eta}.$$

In the semiclassical limit of large eikonals, i.e., $kf \gg 1$, Eq. (2.16) gives the normalization constant $\mathcal{N}_{\omega,0}$ as

$$\mathcal{N}_{\omega,0} = \frac{2\pi}{k} \frac{\partial n}{\partial x}(\omega, x = 0). \quad (3.6)$$

Therefore, expanding $n(\omega, x)$ around $x = 0$, we obtain the linear approximation to Eq. (3.6), i.e.,

$$n(\omega, x) = \frac{kf}{\pi} - \frac{1}{2} + x \frac{\partial n}{\partial x}(\omega, x = 0), \quad (3.7)$$

where

$$\frac{\partial n}{\partial x}(\omega, x = 0) = \frac{2\mathcal{S}(kf)}{\pi^2}, \quad (3.8)$$

and the stability function

$$\mathcal{S}(u) = \int_0^u dy \frac{\sin^2 y}{y}, \quad (3.9)$$

which has the asymptotic behavior

$$\mathcal{S}(u) \xrightarrow{u \gg 1} \frac{1}{2} \left[\ln(2u) + \gamma - \frac{\sin 2u}{2u} \right] + O(u^{-2}),$$

$$\mathcal{S}(u) \xrightarrow{u \ll 1} \frac{u^2}{2} + O(u^4), \quad (3.10)$$

where $\gamma = 0.5772156649015328606$ is the Euler constant [22]. The accuracy of this linear approximation can be appreciated in Fig. 2, in which the scaled separation constant α/k is depicted as a function of the scaled focal length kf . It is apparent that, in range of values of α that contribute significantly to the decay rate in Eq. (3.2), the linear approximation

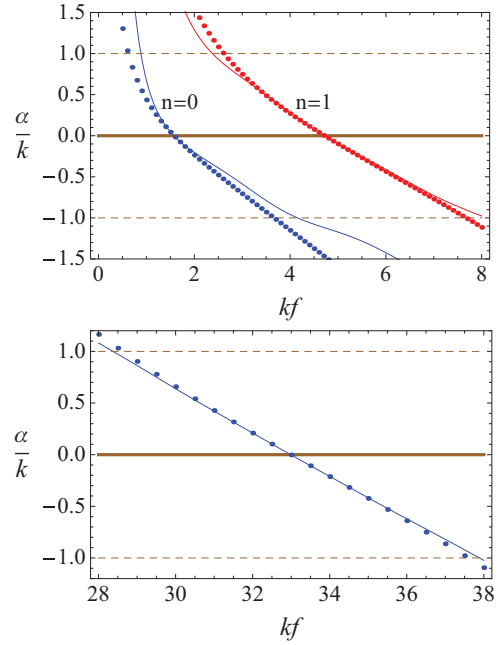


FIG. 2. (Color online) Quantization of the separation constant $\alpha_n(\omega)$ as a function of the focal length f of the parabola: exact (dots) and analytical (full curves) results for $n = 0$ and $n = 1$ (upper figure) and for $n = 10$ (lower figure). It is apparent from the upper figure that within the range of separation constants contributing significantly to the spontaneous decay rate, i.e., $\alpha_n(\omega)/k \in (-1, 1)$ (dashed horizontal lines), the analytical approximation in Eq. (3.7) is satisfactory even for the lowest possible values of the quantum number n .

is quite a satisfactory description, even in the range of small quantum numbers n .

Moreover, by using the integral

$$\int_{-\infty}^{\infty} dx \frac{x^2}{\sinh^2 x} e^{i\beta x/\pi} = \pi^2 \frac{(\beta/2) \coth(\beta/2) - 1}{\sinh^2(\beta/2)}, \quad (3.11)$$

we finally obtain in this linear approximation

$$\frac{\Gamma(\omega_0)}{\Gamma_s(\omega_0)} = 1 + 2 \sum_{M=1}^{\infty} 3 \cos[2M(u - \pi/2)] \times \frac{2M\mathcal{S}(u) \coth[2M\mathcal{S}(u)] - 1}{\sinh^2[2M\mathcal{S}(u)]} \Big|_{u=k_0 f}. \quad (3.12)$$

This result allows for a straightforward and elegant interpretation. The first term on the right-hand side accounts for the free-space spontaneous decay rate. The terms with $M > 0$ size up the boundary effects and can be attributed to the repeated reflections of the emitted photon at the parabolic mirror, with M counting the number of reflections. This is noticeable from the characteristic phase factors in Eq. (3.12), which appear in integer multiples of the classical eikonal $2k_0 f$ characterizing a photon traveling from the focus, along the symmetry axis, to the mirror and back again.

With each of those closed orbits an additional phase shift of π is attached, which is equivalent to a Maslov index 2 [28]. The corresponding amplitude is given by the integer multiple M of the factor $2\mathcal{S}(k_0 f)$ that specifies the stability of the classical trajectories.

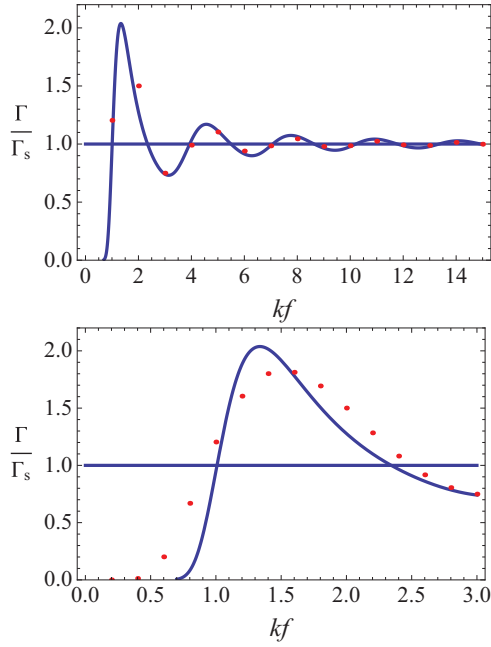


FIG. 3. (Color online) Scaled spontaneous decay rate $\Gamma(\omega_0)/\Gamma_s(\omega_0)$ as a function of the scaled focal length $k_0 f$ of the parabola with $k = \omega_0/c$: exact results of Eq. (3.2) (dots), semiclassical results (solid) of Eq. (3.12) (we also indicate the free-space value as a horizontal line).

The dependence of $\Gamma(\omega_0)$ on f is shown in Fig. 3. It is clear that in the limit of large focal lengths ($k_0 f \gg 1$), $\Gamma(\omega_0)$ eventually tends to its free-space value $\Gamma_s(\omega_0)$ in an oscillatory manner. These oscillations evidence the presence of the parabolic cavity and are satisfactorily described by the M terms in Eq. (3.12).

It is also patent from Fig. 3 that this approximation also yields remarkably accurate results even for smaller focal lengths with $k_0 f < 1$, as long as $n(\omega_0, x=0) \geq 0$. Furthermore, we also recognize from Eq. (3.12) that $\Gamma(\omega_0)$ vanishes when $k_0 f \ll 1$. This reflects that in those cases the cavity is so small that, at the frequency ω_0 , effectively only the field mode with separation constant $\alpha_{n=0}(\omega_0)$ is coupled dominantly to the two-level dipole. From Fig. 2 one can conclude that $\alpha_{n=0}(\omega_0)$ tends to infinity for $k_0 f \ll 1$, so the factor $[\pi \alpha_n(\omega_0)/k_0]^2 / [\sinh(\pi \alpha_n(\omega_0)/k_0)]^2$ in Eq. (3.2) tends exponentially to zero. This situation is in extreme contrast to the spontaneous photon emission in free space.

B. Dynamics of the spontaneous decay

We next investigate the dynamics of the spontaneous photon emission in more detail, to elucidate under which conditions it can be properly described by an exponential decay.

In the dipole and rotating-wave approximations, the time evolution of the spontaneous decay is determined by the time-dependent Schrödinger equation with the Hamiltonian (2.7) and the initial condition (2.8). Taking advantage of the explicit form of the semiclassical mode functions of Sec. II B, the interaction Hamiltonian (2.6) can be rewritten in the equivalent

form

$$\hat{H}_{AF} = \sum_n \int_0^\infty d\omega c_{\omega,n}^* |e\rangle \langle g| \hat{a}_{\omega,n} + \text{H. c.} \quad (3.13)$$

Here, the coupling constants are

$$c_{\omega,n} = i \sqrt{\frac{2\pi\hbar c}{\omega \mathcal{N}_{\omega,n}}} \mathcal{D}(x_n), \quad (3.14)$$

with $x_n = c\pi\alpha_n(\omega)/\omega$, and

$$\mathcal{D}(x) = \sqrt{\frac{3}{\pi^2} \frac{x^2}{\sinh^2 x} \frac{\hbar\Gamma_s(\omega)}{2\pi}}. \quad (3.15)$$

In terms of these quantities, the free-space spontaneous decay rate can also be recast as

$$\Gamma_s(\omega_0) = \frac{2\pi}{\hbar^2} \int_0^\infty dn |c_{\omega_0,n}|^2 = \frac{2\pi}{\hbar} \int_{-\infty}^\infty dx |\mathcal{D}(x)|^2. \quad (3.16)$$

Consistently with the rotating-wave approximation, we have that $\Gamma_s(\omega_0) \ll \omega_0$.

For our initial conditions, we can write down

$$|\psi(t)\rangle = A_e(t)|e\rangle|0\rangle + \sum_n \int_0^\infty d\omega A_{\omega,n}(t)|g\rangle \hat{a}_{\omega,n}^\dagger |0\rangle, \quad (3.17)$$

and the resulting Schrödinger equation can be solved with the help of a Laplace transformation to get

$$A_{\omega,n}^{(\pm)}(t) = \pm \frac{1}{2\pi} \int_{-\infty \pm i0}^{\infty \pm i0} d\Lambda e^{-i\Lambda t/\hbar} e^{-iE_g t/\hbar} \frac{c_{\omega,n}}{\Lambda - \hbar\omega} \frac{i}{f(\Lambda)}, \quad (3.18)$$

$$A_e^{(\pm)}(t) = \pm \frac{1}{2\pi} \int_{-\infty \pm i0}^{\infty \pm i0} d\Lambda e^{-i\Lambda t/\hbar} e^{-iE_g t/\hbar} \frac{i}{f(\Lambda)},$$

with

$$f(\Lambda) = \Lambda - \hbar\omega_0 - \Sigma(\Lambda), \quad (3.19)$$

and $\Sigma(\Lambda)$ being the self-energy of the two-level system, viz.,

$$\Sigma(\Lambda) = \sum_n \int_0^\infty d\omega \frac{|c_{\omega,n}|^2}{\Lambda - \hbar\omega}. \quad (3.20)$$

The \pm signs refer to the retarded (+) and advanced (−) solutions valid for $\text{sgn}(t) = \pm 1$. The notation $\pm i0$ indicates that the integration has to be performed in the complex Λ plane parallel to the real axis with an infinitesimal positive (+) or negative (−) imaginary offset.

1. The self-energy in the semiclassical approximation

To perform the Λ integrations in Eqs. (3.18), we have first to determine the Λ dependence of the self-energy function $f(\Lambda)$ in the region around $\Lambda \approx \hbar\omega_0$. To achieve this, we re draft Eq. (3.20) with the help of the Poisson summation formula as

$$\Sigma(\Lambda) = - \sum_{M=-\infty}^{\infty} \int_{-\infty}^{\infty} dx \times \int_0^\infty d\omega \frac{\partial n(\omega, x)}{\partial x} \frac{|c_{\omega n}|^2}{\hbar\omega - \Lambda} e^{i2\pi M n(\omega, x)}. \quad (3.21)$$

Thereby, we have used the smooth real-valued function $n(\omega, x)$ given by Eq. (3.7). The imaginary part of $n(\omega, x)$ tends to plus (minus) infinity for large ω with a positive (negative) imaginary part, whence we obtain the semiclassical approximation

$$\Sigma^\pm(\Lambda) = \Sigma(\Lambda \pm i0) = \hbar\delta\omega \mp i \frac{\hbar\Gamma_s(\Lambda/\hbar)}{2} \times \left[1 + \frac{6}{\pi^2} \sum_{M=1}^{\infty} \int_{-\infty}^{\infty} dx \frac{x^2}{\sinh^2 x} e^{\pm i2\pi Mn(\Lambda/\hbar, x)} \right], \quad (3.22)$$

for real values of Λ . Herein, $\delta\omega$ is the resonant contribution of the Lamb shift of the two-level transition $|g\rangle \rightarrow |e\rangle$ originating from the real part of the $M=0$ contribution in Eq. (3.21). Henceforth, we assume that this contribution is incorporated in a renormalized transition frequency ω_0 in which the complete Lamb shift is taken into account in second-order perturbation theory [29].

The contribution of a particular value of $M \geq 1$ in Eq. (3.22) can be attributed to M reflections of a photon path at the parabolic mirror; each photon path being associated with a particular value of the separation constant $x \in (-\infty, \infty)$.

By adopting the approximation (3.22), the Λ integration in Eqs. (3.18) can be performed in two complementary ways. In the dressed-state representation, this integration is evaluated using residue calculus. Alternatively, this can be directly performed with the help of a photon-path representation of the integrand. In what follows, we scrutinize both options.

2. The dressed-state representation in the pole approximation

The poles of the integrands in Eq. (3.18) [which stem from the zeros of $f(\Lambda)$] yield the complex-valued dressed energies of the strongly-coupled atom-field system. The time dependent quantum state (3.17) can thus be expressed as a sum of contributions of all these dressed states.

In all these Λ integrations the dominant contributions are expected to arise from values of $\Lambda \approx \hbar\omega_0$. According to Eq. (3.22), the characteristic values of the self-energy $\Sigma^\pm(\Lambda)$ are of the order of $O(\hbar\Gamma_s(\Lambda/\hbar))$. Therefore, as long as the self-energy is a slowly varying function of Λ around $\Lambda \approx \hbar\omega_0$, i.e., whenever

$$\hbar\Gamma_s(\omega_0) \left| \frac{\partial \Sigma^\pm(\Lambda)}{\partial \Lambda} \right|_{\Lambda=\hbar\omega_0} \ll 1, \quad (3.23)$$

we can approximate $\Sigma^\pm(\Lambda)$ by its value at $\Lambda = \hbar\omega_0$. In this case, the equation $f(\Lambda) = 0$ has only one solution, namely,

$$\Lambda_0 = \hbar\omega_0 + \Sigma^\pm(\hbar\omega_0). \quad (3.24)$$

In this pole approximation [25], the dressed-state representation (3.18) reads

$$A_e^{(\pm)}(t) = e^{-i[E_g + \hbar\omega_0 + \Delta(\omega_0)]t/\hbar} e^{-|t|\Gamma(\omega_0)/2}, \quad (3.25)$$

for both the retarded ($t \in [0, \infty)$) and advanced ($t \in (-\infty, 0]$) dynamics of the state $|e\rangle$. The quantity $\Delta(\omega_0) = \text{Re}[\Sigma^\pm(\hbar\omega_0)]$ represents the resonant energy shift induced by the spontaneous emission. Equation (3.25) hints at an exponential decay of the probability amplitude $A_e(t)$, with a rate $\Gamma(\omega_0)$. This is a consequence of the rotating-wave approximation, which involves an averaging over times scales of the order of

$1/\omega_0$. At very short times (say, of the order of $1/\omega_0$ or less), this pole approximation breaks down and deviations from an exponential decay may occur [30].

From the linear estimate (3.7) we conclude that the semiclassical approximation (3.22) is valid as long as $k_0 f \gg 1$, so that many modes are excited by the spontaneous emission. In addition, f must also be small enough so that inequality (3.23) is fulfilled. This latter condition implies $f \ll c/\Gamma_s(\omega_0)$ and states that the focal length still has to be significantly smaller than the typical length $\Delta l = c/\Gamma_s(\omega_0)$ of the spontaneously generated photonic wave packet in free space. Physically speaking, this condition implies that the repeated reflections of the photon wave packet at the parabola overlap significantly in space-time, so that they cannot be resolved and thus interfere. This interference gives rise to the oscillations of the spontaneous decay rate $\Gamma(\omega_0)$, which have already been investigated in subsection III A.

3. The semiclassical photon-path representation

As soon as the smoothness condition (3.23) is no longer fulfilled, the Λ integrations in Eqs. (3.18) have to be evaluated by more sophisticated means. According to our previous considerations, this happens if the focal length is so large that $f > c/\Gamma_s(\omega_0)$. In this instance, the contributions from the repeated reflections of the photon at the parabola are separated sufficiently well in space-time, so that they can be distinguished by appropriate measurements.

In this regime, a systematic photon-path representation of the amplitude $A_e^{(\pm)}(t)$ is convenient not only from the computational, but also from the physical point of view. In the spirit of the path-integral approach, $A_e^{(\pm)}(t)$ can be appropriately represented as a sum of amplitudes associated with all photon paths which start and end at the position of the two-level system and which are reflected repeatedly at the cavity.

To obtain that representation, we start from the semiclassical approximation of the self-energy given in Eq. (3.22). After some direct computations, one gets

$$\begin{aligned} \frac{1}{f(\Lambda \pm i0)} &= \frac{1}{f_0(\Lambda \pm i0)} \pm i2\pi \frac{1}{f_0(\Lambda \pm i0)} \int_{-\infty}^{\infty} dx_1 \\ &\times \int_{-\infty}^{\infty} dx_2 \mathcal{D}(x_1) \mathcal{Y}^\pm(x_1, x_2) e^{\pm i2\pi n(\Lambda/\hbar, x_2)} \\ &\times \mathcal{D}(x_2) \frac{1}{f_0(\Lambda \pm i0)}, \end{aligned} \quad (3.26)$$

where

$$\begin{aligned} f_0(\Lambda \pm i0) &= \Lambda - \hbar\omega_0 \pm i \frac{\hbar\Gamma_s(\Lambda/\hbar)}{2}, \\ \mathcal{Y}^\pm(x_1, x_2) &= -\delta(x_1 - x_2) \\ &+ \int_{-\infty}^{\infty} dx_3 \mathcal{Y}^\pm(x_1, x_3) e^{\pm i2\pi n(\Lambda/\hbar, x_3)} S^\pm(x_3, x_2), \end{aligned} \quad (3.27)$$

and the scattering S matrix given by

$$S^\pm(x_3, x_2) = \delta(x_3 - x_2) \mp 2i\pi \mathcal{D}(x_3) \frac{1}{f_0(\Lambda \pm i0)} \mathcal{D}(x_2). \quad (3.28)$$

Let us set out the (generalized) basis vectors $\{|x\rangle\}$ in the Hilbert space of square-integrable functions of the separation constant $x \in \mathbb{R}$. Using Eq. (3.15) and defining the dipole vector $|\mathcal{D}\rangle$ by

$$|\mathcal{D}\rangle := \int_{-\infty}^{\infty} dx \mathcal{D}(x)|x\rangle, \quad \langle \mathcal{D}| := \int_{-\infty}^{\infty} dx \mathcal{D}(x)\langle x|, \quad (3.29)$$

Eq. (3.26) can be conveniently recast as

$$\begin{aligned} \frac{1}{f(\Lambda \pm i0)} &= \frac{1}{f_0(\Lambda \pm i0)} \mp i2\pi \frac{1}{f_0(\Lambda \pm i0)} \\ &\times \sum_{M=0}^{\infty} \langle \mathcal{D}|(e^{\pm i2\pi n(\Lambda/\hbar)} \mathbf{S}^{\pm})^M e^{\pm i2\pi n(\Lambda/\hbar)} |\mathcal{D}\rangle \\ &\times \frac{1}{f_0(\Lambda \pm i0)}, \end{aligned} \quad (3.30)$$

$$\begin{aligned} A_e^{(\pm)}(t) &= e^{-i(E_g/\hbar + \omega_0)t - |t|\Gamma_s(\omega_0)/2} + \sum_{M=1}^2 \Theta(|t| - MT) e^{-i(E_g/\hbar + \omega_0)t} e^{\pm i2\pi Mn(\omega_0, x=0)} \\ &\times \sum_{k=0}^{M-1} \binom{M-1}{k} \frac{(-1)^{k+1}}{(k+1)!} [(|t| - MT)\Gamma_s(\omega_0)]^{k+1} e^{-(|t| - MT)\Gamma_s(\omega_0)/2} \\ &\times \left(\int_{-\infty}^{\infty} dx \frac{3x^2}{\pi^2 \sinh^2 x} e^{\pm ix2\pi(M-k)(\partial n/\partial x)(\omega_0, x=0)} \right) \left(\int_{-\infty}^{\infty} dx \frac{3x^2}{\pi^2 \sinh^2 x} e^{\pm ix2\pi(\partial n/\partial x)(\omega_0, x=0)} \right)^k + \dots \end{aligned} \quad (3.33)$$

In this expression

$$T := 2\pi\hbar \frac{\partial n(\omega_0, x=0)}{\partial \Lambda} = \frac{2f}{c} \quad (3.34)$$

is the classical period of the closed photon path with separation constant $x = 0$, which starts at the focus of the parabola and extends along the symmetry axis to the vertex and back again.

The various terms appearing in Eq. (3.33) allow again for a sensible interpretation. In the retarded solution (+), for example, the very first term on the right-hand side expresses the spontaneous decay process of the excited state $|e\rangle$ in the absence of the cavity and is governed by free-space decay rate $\Gamma_s(\omega_0)$. The remaining terms with $M \geq 1$ describe the time dependence of the probability amplitudes for the photon after M reflections. The M th contribution represents a process in which a photon is emitted at time $t = 0$ and is reabsorbed again at a time $t \geq MT$. This photon accumulates a phase of $2\pi Mn(\omega_0, x = 0)$, which is the eikonal associated with the classical path with separation constant $x = 0$. Furthermore, the photon can be scattered $0 \leq k \leq (M - 1)$ times during its intermediate returns to the focus of the parabolic cavity.

The stability of the path with $x = 0$ is described by the characteristic quantity $\partial n/\partial x(\omega_0, x = 0)$ [compare with Eq. (3.9)]. If this path were stable, i.e., $\partial n/\partial x(\omega_0, x = 0) = 0$, the representation (3.33) would reduce to previous results for a spherically symmetric cavity, in which all relevant photon paths are stable and their contributions add up in phase [13].

As far as the time evolution of $A_e^{(\pm)}(t)$ is concerned, two different regimes may be distinguished. If the classical period is significantly smaller than the free-space decay, i.e.,

with the scattering operator

$$\mathbf{S}^{\pm} = \mathbb{1} \mp 2i\pi |\mathcal{D}\rangle \frac{1}{f_0(\Lambda \pm i0)} \langle \mathcal{D}|. \quad (3.31)$$

The quantity

$$e^{\pm i2\pi n(\Lambda/\hbar)} = \int_{-\infty}^{\infty} dx |x\rangle \langle x| e^{\pm i2\pi n(\Lambda/\hbar, x)} \quad (3.32)$$

encodes the phase accumulated by a photon during all closed paths starting and ending at the focus.

For sufficiently large focal lengths f , for which the pole approximation is not applicable but for which the linear approximation still applies, $A_e^{(\pm)}(t)$ can be evaluated term by term with the help of Eq. (3.30). The contributions with $M \leq 2$, for example, are explicitly given by

$T = 2f/c \ll 1/\Gamma_s(\omega_0)$, the probability amplitudes associated with different photon bounces $M \geq 1$ overlap in time significantly and cannot be distinguished in the evolution. In this case, $A_e^{(\pm)}(t)$ leads to an exponential decay with the modified rate $\Gamma(\omega_0)$, which has been discussed in detail in Eqs. (3.2) and (3.12). In the opposite limit of long classical periods, i.e., $T = 2f/c \gg 1/\Gamma_s(\omega_0)$, the contributions associated with different returns $M \geq 1$ are well separated in time and the overall time evolution of $A_e^{(\pm)}(t)$ is modified significantly.

The time evolution of the probability $|A_e^{(\pm)}(t)|^2$ is depicted in Fig. 4. For typical free-space decay rates of the order of 10^9 s^{-1} , focal lengths significantly larger than 10 cm would be required. Furthermore, in view of the stability properties of the photon path with $x = 0$, already for small values of the quantization number n the contributions of repeated returns of the photon with $M \geq 1$ are suppressed significantly. So, in view of current technological capabilities, the experimental observation of the modified spontaneous decay as described by Eq. (3.33) is challenging.

To sum up this discussion, with the present values in our experimental setup (focal length $f = 2.1 \text{ mm}$ and wavelength of 369 nm), one can reach the typical condition for strong coupling. It follows then that there should be several phenomena which can be observed in this limit, as reviewed in Ref. [31].

IV. PHOTON DYNAMICS

Although the mean values of the electric and magnetic field strengths vanish for any one-photon state, their fluctuations may be seen as stemming from an effective one-photon

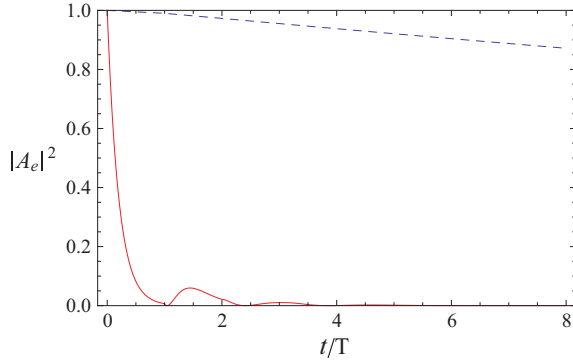


FIG. 4. (Color online) Time evolution of the probability $|A_e^{(\pm)}(t)|^2$. The interaction time t is plotted in units of the classical period T of the photon path connecting the two-level system at the focus of the parabola with its vertex. The parameters are $n = k_0 f/\pi - 1/2 = 0$, $\Gamma_s(\omega_0)T = 0.01$ (dashed curve), and $\Gamma_s(\omega_0)T = 5$ (full curve).

amplitude. In the long-time limit, this latter amplitude consists of an asymptotic wave propagating along the symmetry axis of the parabola with a characteristic transversal spatial modulation and polarization pattern and of a spherically outgoing wave whose amplitude vanishes far from the focus of the parabola. The multiple reflections of the spontaneously emitted photon manifest themselves in the transversal spatial modulations.

An especially interesting quantity to ascertain the dynamics of this single-photon state is the normally-ordered electric-field correlation function. Taking into account the time evolution in Eq. (3.17), we can write [32]

$$\begin{aligned} \langle \psi(t) | : \hat{E}_k(\mathbf{x}) \hat{E}_\ell(\mathbf{x}) : | \psi(t) \rangle \\ = (\mathbf{e}_k \cdot \nabla \times \mathbf{F}^\pm(\mathbf{x}, t)) (\mathbf{e}_\ell \cdot \nabla \times \mathbf{F}^{\pm*}(\mathbf{x}', t)) + \text{c. c.}, \end{aligned} \quad (4.1)$$

where \mathbf{e}_k and \mathbf{e}_ℓ are Cartesian unit vectors and the effective one-photon amplitude reads

$$\mathbf{F}^\pm(\mathbf{x}, t) = -i \sum_n \int_0^\infty d\omega \sqrt{\frac{\hbar\omega}{2\epsilon_0}} A_{\omega,n}^{\pm*}(t) \mathbf{G}_{\omega,n}^*(\mathbf{x}). \quad (4.2)$$

According to Glauber's theory [33], this (and analogous normally-ordered higher-order correlation functions) can be measured by optical photodetection.

In general, the one-photon amplitude (4.2) has to be evaluated numerically. However, we can grasp its basic space-time dependence, if we concentrate on the long-time limit $\Gamma(\omega_0)|t| \gg 1$, for which

$$A_{\omega,n}^{(\pm)}(t) = e^{-i\omega t} e^{-iE_g t/\hbar} \frac{c_{\omega,n}}{\hbar(\omega - \omega_0) - \Sigma^\pm(\hbar\omega)}, \quad (4.3)$$

where we have used Eq. (3.18) and neglected exponentially small terms. Provided the semiclassical relation (2.16) is applicable, the one-photon amplitude (4.2) can be rewritten, using the Poisson summation formula, as a sum of all possible photon paths originating at the focus, i.e.,

$$\mathbf{F}^\pm(\mathbf{x}, t) = -\mathbf{e}_\varphi \sum_{M=-\infty}^{\infty} \int_0^\infty d\omega \int_{-\infty}^{\infty} dx \frac{x}{\sinh x} \sqrt{\frac{3\Gamma_s(\omega)\hbar^3\omega}{16\epsilon_0 c \pi^5}} \frac{\chi_{\omega,n}(\xi)}{\sqrt{\xi}} \frac{\chi_{\omega,n}(\eta)}{\sqrt{\eta}} e^{i(\omega+E_g/\hbar)t} \frac{e^{i2\pi M n(\omega,x)}}{\hbar(\omega - \omega_0) - \Sigma^\mp(\hbar\omega)}. \quad (4.4)$$

The dominant contribution to the integral over x comes from a small neighborhood around $x = 0$, so we can use the linear approximation (3.7) for $n(\omega, x)$. Besides, in the radiation zone, i.e., far from the focus of the parabola, the mode functions $\chi_{\omega,n}(\xi)$ and $\chi_{\omega,n}(\eta)$ can be replaced by their asymptotic expressions (see the Appendix). Finally, if the focal length f is not too large, i.e., $2f\Gamma(\omega_0)/c \ll 1$, the ω integration can be performed with the pole approximation. With all this in mind, the final result turns out to be

$$\begin{aligned} \mathbf{F}^\pm(\mathbf{x}, t) = \pm i \frac{\mathbf{e}_\varphi}{\sqrt{\xi\eta}} \sqrt{\frac{3\Gamma_s(\omega_0)\hbar c}{4\epsilon_0 \pi^5 \omega_0}} e^{iE_g t/\hbar} \sum_{M \geq 0} e^{\mp i 2\pi M n(\omega_0, x=0)} \\ \times \left\{ \Theta \left(\left| t \right| - \frac{\xi + \eta}{2c} - MT \right) \frac{\pi^2 e^{\pm i\omega_0[|t| - (\xi + \eta)/(2c)]} e^{-\Gamma(\omega_0)[|t| - (\xi + \eta)/(2c)]/2}}{2 \cosh^2[-\ln \sqrt{\xi/\eta} + 2M\mathcal{S}(k_0 f)]} \right. \\ \left. - \Theta \left(\left| t \right| - \frac{\xi - \eta}{2c} - MT \right) \frac{\pi^2 e^{\pm i\omega_0[|t| - (\xi - \eta)/(2c)]} e^{-\Gamma(\omega_0)[|t| - (\xi - \eta)/(2c)]/2}}{2 \cosh^2[-\ln \sqrt{\eta\xi/(2f)^2} + 2(M-1)\mathcal{S}(k_0 f)]} \right\}. \end{aligned} \quad (4.5)$$

In the derivation of Eq. (4.5), we have used the relation

$$\int_{-\infty}^{\infty} dx \frac{x}{\sinh x} e^{i\beta x/\pi} = \frac{\pi^2}{2 \cosh^2(\beta/2)}, \quad (4.6)$$

and we have neglected exponentially small terms. In the limit $\Gamma(\omega_0)2f/c \ll 1$, which we are considering here, the unit step functions $\Theta(u)$ associated with different M values have almost identical support. For $\mathcal{S}(\omega_0 f/c) \gg 1$, in Eq. (4.5) only contributions with $M = 0$ for the first term in curly brackets and with $M = 1$ for the second term in curly brackets are significant

so that the one-photon amplitude simplifies to

$$F^\pm(\mathbf{x}, t) = \pm i \mathbf{e}_\varphi \sqrt{\frac{3\Gamma_s(\omega_0)\hbar c}{16\epsilon_0\pi\omega_0}} e^{iE_g t/\hbar} \left(\Theta(|t| - r/c) e^{\pm i\omega_0(|t|-r/c)} e^{-\Gamma(\omega_0)(|t|-r/c)/2} \frac{\rho}{r^2} - \Theta(|t| - z/c - T) e^{\pm i\omega_0(|t|-z/c)} e^{-\Gamma(\omega_0)(|t|-z/c)/2} e^{\mp i2\pi n(\omega_0, x=0)} \frac{2}{f} \frac{\rho/(2f)}{\{1 + [\rho/(2f)]^2\}^2} \right). \quad (4.7)$$

This expression could also be obtained by evaluating the one-photon amplitude directly with the help of multidimensional Jeffreys-Wentzel-Kramers-Brillouin (JWKB) methods [28]. This indicates that the residual terms in Eq. (4.5) can be attributed to diffraction phenomena and to photon scattering by the atom. In particular, these contributions become important for values of the stability function $\mathcal{S}(k_0 f)$ of the order of unity.

Starting from Eq. (4.5), it is straightforward to demonstrate that in an asymptotic plane $z \rightarrow \infty$, the photon transversal energy density is

$$\int_{-f}^{\infty} dz \frac{\epsilon_0}{2} \langle \psi(t) | : \hat{\mathbf{E}}^2(\mathbf{x}) + c^2 \hat{\mathbf{B}}^2(\mathbf{x}) : | \psi(t) \rangle = \hbar\omega_0 I(y), \quad (4.8)$$

with $y = [\rho/(2f)]^2$ and with the planar energy distribution

$$I(y) = \frac{\Gamma_s(\omega_0)}{\Gamma(\omega_0)} \frac{1}{4\pi f^2} \left\{ 6 \frac{y}{(1+y)^4} + 12 \sum_{M=1}^{\infty} \cos[2M(k_0 f - \pi/2)] \frac{y e^{2Mv}}{(1+y)^2 (e^{2Mv} + y)^2} \right\}, \quad (4.9)$$

with $v = 2\mathcal{S}(k_0 f)$. With the help of Eq. (3.12) one can easily check that

$$\int_0^{2\pi} d\varphi \int_0^{\infty} d\rho \rho I(y) = 1, \quad (4.10)$$

consistent with the fact that, within the rotating-wave approximation, the total energy of the one-photon state is $\hbar\omega_0$.

According to Eq. (4.9), the terms with $M \geq 1$ contribute the most when the quantization condition $k_0 f = \pi(n + 1/2)$ is fulfilled for $n \in \mathbb{N}$. In Fig. 5 the transversal energy distribution is depicted for the frequencies corresponding to the two lowest integer quantization values $n = 0$ and $n = 1$. For $n = 0$, the contributions of repeated reflections at the parabolic boundary slightly modify the transversal energy distribution. However, already for $n = 1$, it turns out that, due to the instability of the photon path determined by the parameter v , the contributions of the terms with $M \geq 1$ are negligible in the transverse energy distribution.

We also point out that we have recently demonstrated the experimental generation of temporal modes allowing for an efficient coupling of single photons and single two-level systems in free space using a deep parabolic mirror [34], which confirms the theory developed here.

V. CONCLUDING REMARKS

We have explored the dynamics of the spontaneous emission by a two-level atom at the focus of a parabolic cavity. Concentrating on the optical regime, we have determined the time evolution of both the atom and the photon in the dipole and rotating-wave approximations. We have investigated also the advanced solution, for it approaches, at a particular time ($t = 0$), a quantum state in which the atom is in its excited state and the field in its ground (vacuum) state. Thus, it describes a physical situation in which the atom is excited with near certainty by a single photon in a multimode scenario.

By taking into account the vectorial character of the electromagnetic field, we have demonstrated that the photon exchange can be described in a physically transparent way with the help of semiclassical methods. Thereby, the observables of interest are represented as sums of probability amplitudes associated with repeated reflections of the photon at the boundary of the parabolic cavity and with its repeated resonant scatterings by the atom. This semiclassical description does not only yield a quantitatively adequate description of this physical exchange in the limit of short wavelengths, but also constitutes a satisfactory approximation in the opposite limit of long wavelengths.

Bearing in mind the current experimental activities aiming at the realization of quantum repeaters, half-open cavities, such as the one discussed in this paper, offer interesting perspectives for coupling an elementary material qubit almost perfectly to the electromagnetic radiation field even in extreme multimode scenarios. Experimental work in that direction is in progress in our laboratory.

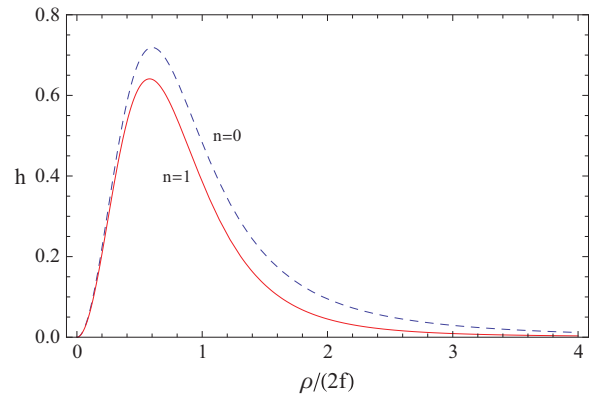


FIG. 5. (Color online) Asymptotic transverse energy distribution $h(\rho/(2f)) = \pi(2f)^2 I(y) \Gamma(\omega_0) / \Gamma_s(\omega_0)$ of the one-photon quantum state for two different values of the quantization constant $n = 0$ (dashed line) and $n = 1$ (full line).

ACKNOWLEDGMENTS

Financial support from the EU FP7 (Grant No. Q-ESSENCE), the BMBF (Project QK_QuOREP), the Spanish DGI (Grant No. FIS2011-26786), and the UCM-BSCH program (Grant No. GR-920992) is acknowledged. It is also a pleasure to thank A. R. P. Rau and M. Sondermann for stimulating discussions. M.S. is supported by the EU 7FP Marie Curie Career Integration Grant No. 322150 ‘‘QCAT’’, NCN Grant No. 2012/04/M/ST2/00789, FNP Homing Plus Project No. HOMING PLUS/2012-5/12 and MNiSW co-financed international Project No. 2586/7.PR/2012/2.

APPENDIX

In this Appendix, details concerning the separation of the vectorial Helmholtz equation in parabolic coordinates and the frequency normalization of the mode functions are summarized.

The parabolic coordinates (ξ, η, ϕ) are defined through

$$x = \sqrt{\xi\eta} \cos \phi, \quad y = \sqrt{\xi\eta} \sin \phi, \quad z = \frac{1}{2}(\xi - \eta), \quad (\text{A1})$$

where $0 \leq \xi, \eta < \infty$, and $0 \leq \phi < 2\pi$. The surfaces $\eta = \text{const}$ are paraboloids of revolution about the positive Z axis, having their focal point at the origin, while the surfaces $\xi = \text{const}$ are directed along the negative Z axis. The plane $z = 0$ corresponds to the condition $\xi = \eta$.

In these coordinates, the Laplacian operator governing the vectorial Helmholtz equation (2.4) is given by

$$\nabla^2 = \frac{4}{\xi + \eta} \left(\frac{\partial}{\partial \xi} \xi \frac{\partial}{\partial \xi} + \frac{\partial}{\partial \eta} \eta \frac{\partial}{\partial \eta} \right) + \frac{1}{\xi\eta} \frac{\partial^2}{\partial \phi^2}. \quad (\text{A2})$$

This implies that mode functions of the form of Eq. (2.11) fulfill Eqs. (2.12). According to Eq. (2.14) these mode functions involve Coulomb functions of zero angular momentum $L, F_0(\mu, \rho)$. We have the asymptotic limit (for large ρ)

$$F_0(\mu, \rho) \sim \sin[\Phi(\mu, \rho)], \quad (\text{A3})$$

with the Coulomb phase

$$\Phi(\mu, \rho) = \rho - \mu \ln(2\rho) + \arg \Gamma(1 + i\mu). \quad (\text{A4})$$

For $|\mu| \ll 1$, the corresponding asymptotic expression reads

$$F_0(\mu, \rho) \sim \rho \sqrt{\frac{e^{\pi\mu} \pi \mu}{\sinh(\pi\mu)}}. \quad (\text{A5})$$

Note that in our case, $\rho = \omega\eta/(2c)$ and $\mu = -\alpha c/\omega$.

If μ is of the order of unity or less, then, consistent with the linear approximation (3.7), the argument

of the Γ function appearing in the Coulomb phase (A4) can be approximated by $\arg \Gamma(1 + i\mu) \simeq -\gamma\mu$, with $\gamma = 0.5772156649015328606 = \lim_{n \rightarrow \infty} (\sum_{k=1}^n 1/k - \ln n)$ denoting Euler’s constant [22].

To determine the frequency normalization factor $\mathcal{N}_{\omega,n}$ of the vector mode functions $\mathbf{g}_{\omega,n}(\mathbf{x}) = \nabla \times \mathbf{G}_{\omega,n}(\mathbf{x})$, we start from the differential identity

$$(\nabla \times \mathbf{A}) \cdot (\nabla \times \mathbf{A}) = \nabla \cdot [\mathbf{A} \times (\nabla \times \mathbf{A})] + \mathbf{A} \cdot [\nabla(\nabla \cdot \mathbf{A}) - \nabla^2 \mathbf{A}], \quad (\text{A6})$$

which is valid for any nonsingular vector field $\mathbf{A}(\mathbf{x})$. Using Gauss’s theorem together with the fact that the mode functions fulfill the relations $\nabla \cdot \mathbf{G}_{\omega,n}(\mathbf{x}) = 0$ and $\mathbf{G}_{\omega,n}(\mathbf{x}) \times \nabla \times \mathbf{G}_{\omega,n}(\mathbf{x})|_{\partial V} = 0$ on the surface of the parabola ∂V , we obtain the normalization condition

$$\int_V d^3\mathbf{x} [\nabla \times \mathbf{G}_{\omega,n}(\mathbf{x})^*] \cdot [\nabla \times \mathbf{G}_{\omega',n'}(\mathbf{x})] = \frac{\omega'^2}{c^2} \int_V d^3\mathbf{x} \mathbf{G}_{\omega,n}(\mathbf{x})^* \cdot \mathbf{G}_{\omega',n'}(\mathbf{x}), \quad (\text{A7})$$

where V denotes the volume bounded by the parabola. The integral on the right-hand side can be evaluated with the help of the one-dimensional differential equations (2.12). In this way, we obtain the relation for $n = n'$, for example,

$$\frac{1}{\sqrt{\omega' \omega_n \mathcal{N}_{\omega',n} \mathcal{N}_{\omega,n}}} W(\chi_{\omega',n}(\xi), \chi_{\omega,n}(\xi)) \int_0^{2f} d\eta \frac{\chi_{\omega',n}(\eta) \chi_{\omega,n}(\eta)}{\eta} = (\omega' - \omega) \frac{\omega' + \omega}{c^2} \int_V d^3\mathbf{x} \mathbf{G}_{\omega',n}(\mathbf{x})^* \cdot \mathbf{G}_{\omega,n}(\mathbf{x}), \quad (\text{A8})$$

with the Wronskian-type quantity

$$W(\chi_{\omega',n}(\xi), \chi_{\omega,n}(\xi)) = \lim_{\xi \rightarrow \infty} \left[\chi_{\omega',n}(\xi) \frac{d\chi_{\omega,n}}{d\xi}(\xi) - \chi_{\omega,n}(\xi) \frac{d\chi_{\omega',n}}{d\xi}(\xi) \right]. \quad (\text{A9})$$

With the help of Eq. (A9), the normalization constant $\mathcal{N}_{\omega,n}$ can be determined in such a way that the frequency normalization condition of Eq. (2.5) is fulfilled. For this purpose we use the following representation of the Dirac δ function

$$\delta(\omega' - \omega) = \lim_{\xi \rightarrow \infty} \frac{\sin[(\omega' - \omega)\xi]}{\pi(\omega' - \omega)}. \quad (\text{A10})$$

This allows us to find the explicit form of the normalization factor given in Eq. (2.14).

[1] *Cavity Quantum Electrodynamics*, edited by P. R. Berman (Academic Press, San Diego, 1994).
 [2] H. Walther, B. T. H. Varcoe, B.-G. Englert, and T. Becker, *Rep. Prog. Phys.* **69**, 1325 (2006).
 [3] S. Haroche and J.-M. Raimond, *Exploring the Quantum: Atoms, Cavities and Photons* (Oxford University Press, Oxford, 2006).
 [4] A. Wallraff, D. I. Schuster, A. Blais, L. Frunzio, R.-S. Huang, J. Majer, S. Kumar, S. M. Girvin, and R. J. Schoelkopf, *Nature (London)* **431**, 162 (2004).

[5] Y. Colombe, T. Steinmetz, G. Dubois, F. Linke, D. Hunger, and J. Reichel, *Nature (London)* **450**, 272 (2007); M. F. Riedel, P. Bhi, Yun Li, T. W. Hänsch, A. Sinatra, and P. Treutlein, *ibid.* **464**, 1170 (2010).
 [6] T. Aoki, B. Dayan, E. Wilcut, W. P. Bowen, A. S. Parkins, T. J. Kippenberg, K. J. Vahala, and H. J. Kimble, *Nature (London)* **443**, 671 (2006); B. Dayan, A. S. Parkins, T. Aoki, E. P. Ostby, K. J. Vahala, and H. J. Kimble, *Science* **319**, 1062 (2008).

- [7] T. Boyer, *Phys. Rev.* **174**, 1764 (1968); K. Kakazu and Y. S. Kim, *Phys. Rev. A* **50**, 1830 (1994); V. V. Klimov, V. S. Letokhov, and M. Ducloy, *ibid.* **56**, 2308 (1997); J. U. Noeckel, G. Bourdon, E. LeRu, R. Adams, I. Robert, J. M. Moison, and I. Abram, *Phys. Rev. E* **62**, 8677 (2000); R. Dubertrand, E. Bogomolny, N. Djellali, M. Lebental, and C. Schmit, *Phys. Rev. A* **77**, 013804 (2008); F. S. S. Rosa, T. N. C. Mendes, A. Tenório, and C. Farina, *ibid.* **78**, 012105 (2008); G. Hétet, L. Slodička, A. Glätzle, M. Henrich, and R. Blatt, *ibid.* **82**, 063812 (2010).
- [8] P. Goy, J. M. Raimond, M. Gross, and S. Haroche, *Phys. Rev. Lett.* **50**, 1903 (1983); R. J. Cook and P. W. Milonni, *Phys. Rev. A* **35**, 5081 (1987); D. J. Heinzen, J. J. Childs, J. E. Thomas, and M. S. Feld, *Phys. Rev. Lett.* **58**, 1320 (1987); F. DeMartini, G. Innocenti, G. R. Jacobovitz, and P. Mataloni, *ibid.* **59**, 2955 (1987).
- [9] I. Gerhardt, G. Wrigge, P. Bushev, G. Zumofen, M. Agio, R. Pfab, and V. Sandoghdar, *Phys. Rev. Lett.* **98**, 033601 (2007); A. N. Vamivakas, M. Atatüre, J. Dreiser, S. T. Yilmaz, A. Badolato, A. K. Swan, B. B. Goldberg, A. Imamoglu, and M. S. Ünlü, *Nano Lett.* **7**, 2892 (2007); G. Zumofen, N. M. Mojarad, V. Sandoghdar, and M. Agio, *Phys. Rev. Lett.* **101**, 180404 (2008); G. Wrigge, I. Gerhardt, J. Hwang, G. Zumofen, and V. Sandoghdar, *Nat. Phys.* **4**, 60 (2008); M. K. Tey, Z. Chen, S. A. Aljunid, B. Chng, F. Huber, G. Maslennikov, and Ch. Kurtsiefer, *ibid.* **4**, 924 (2008); L. Slodička, G. Hétet, S. Gerber, M. Henrich, and R. Blatt, *Phys. Rev. Lett.* **105**, 153604 (2010); Y. Wang, J. Minář, L. Sheridan, and V. Scarani, *Phys. Rev. A* **83**, 063842 (2011).
- [10] S. J. van Enk and H. J. Kimble, *Phys. Rev. A* **63**, 023809 (2001); H. P. Urbach and S. F. Pereira, *Phys. Rev. Lett.* **100**, 123904 (2008).
- [11] I. M. Basset, *J. Mod. Opt.* **33**, 279 (1986); S. J. van Enk, *Phys. Rev. A* **69**, 043813 (2004); N. Bokor and N. Davidson, *Opt. Lett.* **29**, 1968 (2004); M. Sondermann, R. Maiwald, H. Konermann, N. Lindlein, U. Peschel, and G. Leuchs, *Appl. Phys. B* **89**, 489 (2007); D. Pinotsi and A. Imamoglu, *Phys. Rev. Lett.* **100**, 093603 (2008).
- [12] S. Quabis, R. Dorn, M. Eberler, O. Glöckl, and G. Leuchs, *Opt. Commun.* **179**, 1 (2000); R. Dorn, S. Quabis, and G. Leuchs, *Phys. Rev. Lett.* **91**, 233901 (2003); S. A. Aljunid, G. Maslennikov, Y. Wang, D. H. Lan, V. Scarani, and Ch. Kurtsiefer, arXiv:1304.3761 [quant-ph].
- [13] G. Alber, *Phys. Rev. A* **46**, R5338 (1992).
- [14] C. Viviescas and G. Hackenbroich, *Phys. Rev. A* **67**, 013805 (2003).
- [15] J.-M. Daul and P. Grangier, *Eur. Phys. J. D* **32**, 181 (2005).
- [16] U. Dörner and P. Zoller, *Phys. Rev. A* **66**, 023816 (2002).
- [17] M. Stobińska and R. Alicki, *Open Syst. Inf. Dyn.* **19**, 1250023 (2012).
- [18] J. Eschner, Ch. Raab, F. Schmidt-Kaler, and R. Blatt, *Nature (London)* **413**, 495 (2001).
- [19] M. Stobińska, M. Sondermann, and G. Leuchs, *Opt. Commun.* **283**, 737 (2010).
- [20] N. Bokor and N. Davidson, *Opt. Commun.* **281**, 5499 (2008).
- [21] R. Maiwald, A. Golla, M. Fischer, M. Bader, S. Heugel, B. Chalopin, M. Sondermann, and G. Leuchs, *Phys. Rev. A* **86**, 043431 (2012).
- [22] *Handbook of Mathematical Functions*, edited by M. Abramowitz and I. A. Stegun (Dover, New York, 1972).
- [23] C. P. Boyer, E. G. Kalnins, and W. Miller, *Nagoya Math. J.* **60**, 35 (1976).
- [24] L. S. Schulman, *Techniques and Applications of Path Integration* (Wiley, New York, 1981).
- [25] V. Weisskopf and E. Wigner, *Z. Phys.* **63**, 54 (1930).
- [26] C. Cohen-Tannoudji, B. Diu, and F. Laloë, *Quantum Mechanics* (Wiley, New York, 1977).
- [27] P. M. Morse and H. Feshbach, *Methods of Theoretical Physics*, (McGraw-Hill, New York, 1953).
- [28] V. P. Maslov and M. V. Fedoriuk, *Semi-Classical Approximation in Quantum Mechanics* (Reidel, Dordrecht, 1981).
- [29] H. A. Bethe, *Phys. Rev.* **72**, 339 (1947); J. Seke, *Nuovo Cimento D* **18**, 533 (1996).
- [30] S. Geltman, *J. Phys. B* **10**, 831 (1977).
- [31] G. Leuchs and M. Sondermann, *J. Mod. Opt.* **60**, 36 (2013).
- [32] M. Stobińska, G. Alber, and G. Leuchs, *Europhys. Lett.* **86**, 14007 (2009).
- [33] R. Glauber, *Phys. Rev.* **130**, 2529 (1963); **131**, 2766 (1963); P. L. Kelly and W. H. Kleiner, *ibid.* **136**, A316 (1964); H. Carmichael, *Lecture Notes in Physics* (Springer, Berlin, 1991), Vol. 18.
- [34] A. Golla, B. Chalopin, M. Bader, I. Harder, K. Mantel, R. Maiwald, N. Lindlein, M. Sondermann, and G. Leuchs, *Eur. Phys. J. D* **66**, 190 (2012).